

Application of numerical simulation of submersed rock-berm structure under anchor collision for structural health monitoring of submarine power cables

Jinho Woo^a, Dongha Kim^b and Won-Bae Na^{*}

Department Ocean Engineering, Pukyong National University, Busan 608-737, Republic of Korea

(Received April 13, 2014, Revised January 2, 2015, Accepted January 11, 2015)

Abstract. Submersed rock-berm structures are frequently used for protection of underwater lifelines such as pipelines and power cables. During the service life, the rock-berm structure can experience several accidental loads such as anchor collision. The consequences can be severe with a certain level of frequency; hence, the structural responses should be carefully understood for implementing a proper structural health monitoring method. However, no study has been made to quantify the structural responses because it is hard to deal with the individual behavior of each rock. Therefore, this study presents a collision analysis of the submersed rock-berm structure using a finite element software package by facilitating the smoothed-particle hydrodynamics (SPH) method. The analysis results were compared with those obtained from the Lagrange method. Moreover, two types of anchors (stock anchor and stockless anchor), three collision points and two different drop velocities (terminal velocity of each anchor and 5 m/s) were selected to investigate the changes in the responses. Finally, the effect of these parameters (analysis method, anchor type, collision point and drop velocity) on the analysis results was studied. Accordingly, the effectiveness of the SPH method is verified, a safe rock-berm height (over 1 m) is proposed, and a gauge point (0.5 m above the seabed) is suggested for a structural health monitoring implementation.

Keywords: SPH method; collision analysis; rock-berm structure; underwater power cable protector; structural health monitoring

1. Introduction

Submarine (or subsea) power cables have been used to transmit electric power from the mainland to an island, which does not have enough electric power generating facilities for the residents. Recent development in ocean renewable energies makes the conventional energy flows in another direction such as offshore wind farms to the mainland. Accordingly, the electric power transmission lines, submarine power cables, become more important. In energy security point of view, the loss of submarine power cables due to a certain environmental or man-made accident may lead to catastrophic events such as significant inconvenience to residents (cutting

*Corresponding author, Professor, E-mail: wna@pknu.ac.kr

^aBK21 Plus Post Doc Fellow, E-mail: skybreaker@pknu.ac.kr

^bGraduate Student, E-mail: namja@hanmail.net

communications, power, and water supplies). For example, in 2010 the submarine power cable linking Shanghai and Shengsi Island, Zhejiang, was fouled and broken completely as a result of ship anchoring. The island lost its power supply for 4 days, and then electricity was only partially restored to about 90,000 residents using diesel generators (Jie and Yao-Tian 2012). Similarly, in 2006, one of two submarine power cables connecting the main Korean Peninsula to Jeju Island was damaged by ship anchoring activities. This event caused a power-supply blackout for the whole of Jeju Island, resulting in severe inconvenience to nearly 570,000 residents and 30,000 tourists. Fortunately, no loss of human life was reported during that period, likely because the outage lasted only 2.5 h during the daytime (Woo *et al.* 2009). However, it was absolutely undesirable because tourism is important to the island, and the power-supply blackout caused a simultaneous suspension of water availability (Yoon and Na 2013a).

Ship anchoring activities, regarded as the major threat to submarine power cables, can be classified into two components— anchor dragging and anchor colliding (Woo and Na 2014). To protect submarine power cables from the threats, more robust structures should be implemented. For example, after the cable fouling in Jeju Island, the conventional matrix type concrete structures have been replaced by more robust reinforced concrete structures – so called tunnel structures. However, it is not desirable to install the robust reinforced concrete structures along the entire cable route because their fabrication and installation cost is high in relatively deep waters. Accordingly, alternative protecting methods have been used for submarine power cables. One of the alternatives is stacking rocks along the cable route. These submersed rocks (hereafter, submerged rock-berm structure) have been frequently used for protecting not only submarine cables but also subsea pipelines.

In structural health monitoring point of view, the submersed rock-berm structure is hard to be monitored because a single or multiple losses of rocks are hardly identified. So far, it seems that pre- or post-accident monitoring has been an option. For example, the International Cable Protection Committee (2009) suggests the use of automatic identification systems (AISs) for vessels, as a pre-accident monitoring tool. Nevertheless, the use of AISs is not applicable to small ships, and their use has not spread rapidly in some developing and even industrialized countries (Coffen-Smout and Herbert 2000, International Cable Protection Committee 2009, Wagner 1995, Yoon and Na 2013b). Post-accident monitoring is also important to quickly recover the damaged cable but it is absolutely desirable to alarm the interaction between anchor and rocks before damaging the cable. Thus, it is highly demanded for the rock and anchor interaction to be monitored through a proper structural health monitoring technique. Relevant recent works in coastal and offshore structures can be found in monitoring deep water floating structures with GPS, vibration, strain, and FBG sensors (Ren and Zhou 2012, Li *et al.* 2014), measuring optical-based three-dimensional dynamic motion for a floating structure (Yi *et al.* 2013a), investigating modal identification of a jacket-type offshore structure (Yi *et al.* 2013b), monitoring rocks with multiplexed FBG and PZT impedance sensors (Yang *et al.* 2008), assessing caisson-type breakwaters (Lee *et al.* 2012, Huynh, *et al.* 2013), and detecting anomalies in underwater pipelines (Na and Kundu 2002, Na and Yoon 2007). However, these studies are not applicable to the submersed rock-berm structures.

Therefore, it is the first step to investigate the transient dynamic behaviors of the submerged rock-berm structure under anchor activities. Then, depending on the transient dynamics, a certain structural health monitoring mechanism can be constructed. This step has been used to develop a nondestructive testing method and structural health monitoring technique. For example, during the development of the impact echo method, numerical simulation was used to investigate the impact

echo response of structures (Kim *et al.* 2008). Starting from a simple wave propagation problem in a plate, Sansalone and Carino (1987) simulated plane defects in plates. They concluded that the results obtained from finite element solutions helped in developing a theoretical basis for utilizing the impact echo method for detecting defects or anomalies in heterogeneous solids such as concrete. Sansalone (1997) summarized the works carried out the importance of using finite element based computer models for simulating the impact echo response of structures. These models permitted them to study transient stress wave propagation in bounded solids with or without defects. Also, Lee *et al.* (2012) and Huynh *et al.* (2013) adopted finite element simulations to develop vibration-based structural health monitoring methods that are suitable for caisson-type structures.

However, it is hard to find any directly related research work because of the difficulty of rock modeling in numerical analyses and simulation in experimental studies. For example, some studies have been performed to report the behavior of tunnel type protective structures under anchor collision and drag because the tunnel type structures are relatively easier than the submerged rock-berm structure to be modeled or tested in the field experiments (Yoon and Na 2013a, Yoon and Na, 2013b). Other relevant studies focused on the stability of berm breakwaters (Corkum and Martin 2004, Tørumet *al.* 2012) and the fracture of rock under explosion and high strain rate loading (Hao and Hao 2013, Zhu *et al.* 2007), which are not directly connected to the submerged rock-berm structure.

Therefore, this study investigates the low velocity impact on the submerged rock-berm structure during anchor collision. For the analysis, a transient finite element dynamic analysis was carried out to capture the dynamic response of the rock-berm particularly by facilitating the smoothed-particle hydrodynamics (SPH) method, which can simulate the individual behavior of each rock. Thus, the use of the SPH method in solids can deal with the larger local distortion than the grid-based Lagrange method. By comparing the analysis results with those obtained from the typical analysis method, so-called Lagrange method, the applicability of the newly adopted SPH is discussed. In addition, the anchor drop heights are intentionally varied from anchor's terminal velocities to 5 m/s to capture how the change in drop height (or colliding velocity) affects the structural response. It should be noted here that two anchor types (stock and stockless) of 2-ton were considered because these types have been frequently used in anchor activities. Also, three collision points are considered to find the variation of the responses according to the collision points. Finally, a safe rock-berm height and a monitoring gauge point are suggested. It should be noted here that the general purpose finite element software, ANSYS AUTODYN, is used for the analyses. Figure 1 show the schematic of the study. Here, the continuous lines indicate the study flow considered and its scope.

2. Materials and methods

2.1 SPH Method

The SPH method was initially developed by Gingold and Monaghan (1977) and Lucy (1977) for astrophysical problems. It has been used in many research fields such as astrophysics, ballistics, volcanology, and oceanography because it is a mesh-free Lagrange method and resolution can easily be adjusted according to variables such as the density. Most initial problems are fluid-related by dividing the fluid into a set of discrete elements (particles). Libersky and Petschek

(1991) extended the SPH method to solid mechanics. The main advantage of SPH in solids is the possibility of dealing with the larger local distortion than grid-based methods; hence, it has been exploited in many applications in solid mechanics such as metal forming, collision, crack growth, fracture, and fragmentation. The detailed description of the SPH method and associated references can be found in the literature (Lin *et al.* 2014). The basic steps used in each calculation cycle are shown in Fig. 2. As indicated, the computation cycle starts from the initial conditions and converges to particle position through the procedures obtaining strain rates, pressure, internal energy, stresses, particle forces, accelerations, and velocities by the indicated mathematical equations, conservation laws, and engineering models.

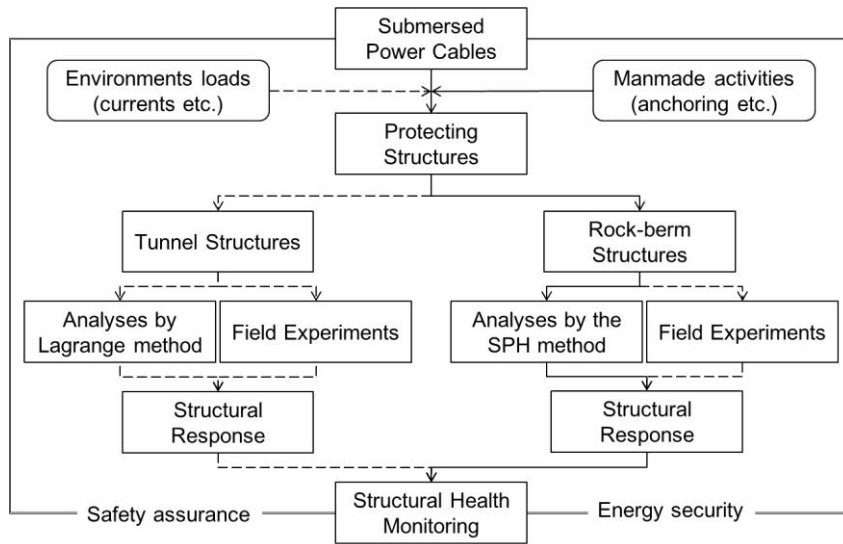


Fig. 1 A schematic of the study flow

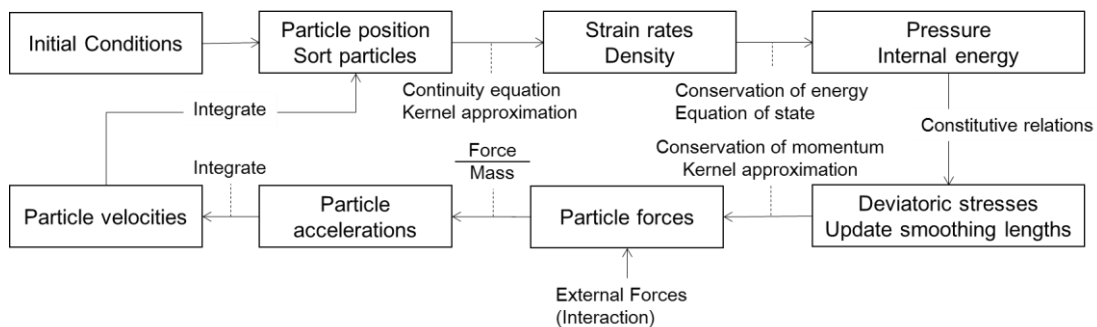


Fig. 2 Computational cycle for the SPH method

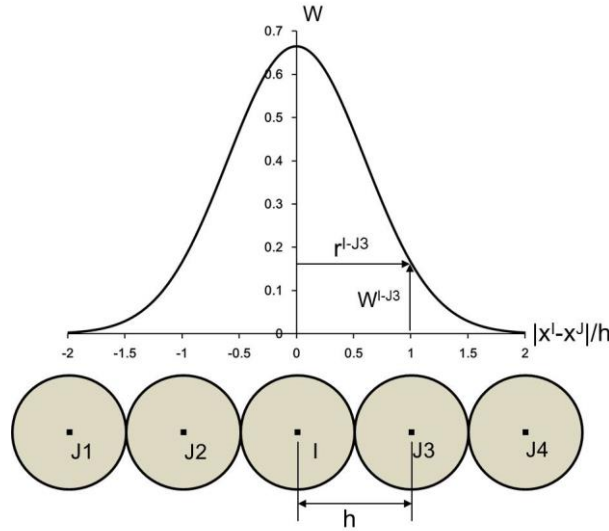


Fig. 3 Schematic of weight function in the SPH method

The SPH method uses kernel approximation, which is based on randomly distributed interpolation points with no assumptions about which points are neighbors, to calculate spatial derivatives and particle density using Kernel estimation (Hayhurst *et al.* 1996). The particle density can be expressed using kernel approximation as follows

$$\rho^I = \sum_{J=1}^N m^J W^{IJ}(x^I - x^J, h) \tag{1}$$

where ρ^I is the density of I -th particle, m^J is the mass of J -th particle, $W^{IJ}(x^I - x^J, h)$ is the weight function according to particle size h . x^I and x^J are x -coordinates of I -th and J -th particle. In the SPH method, the particle density can be obtained as mass of neighbor particle multiplied by a weight function. Fig. 3 shows a schematic of the weight function in the SPH method. In the study, the Kernel B-spline is used as the weight function. The basic form of the weight function is as follows

$$W(u) = \begin{cases} 1 - 6u^2 + 6u^3 & 0 \leq u \leq 1/2 \\ 2(1 - u)^3 & \frac{1}{2} < u \leq 1 \\ 0 & u > 1 \end{cases} \tag{2}$$

where u is a parametric variable defined by $u = |x^I - x^J|/(2h)$.

The contact conditions were considered, as shown in Fig. 4. First, the interface between rock and other materials (basement and anchor) is based on the contact algorithms used in Lagrange-oriented finite element codes. Second, the interface between the stones (particle and particle contact) is based on the meshless approach (Seo and Min 2006). If other material intersects the circle of a particle, then contact is assumed to be occurred. When contact occurs, the restoring force is applied along the normal to the surface. In the particle to particle contact, restoring forces are applied between particles.

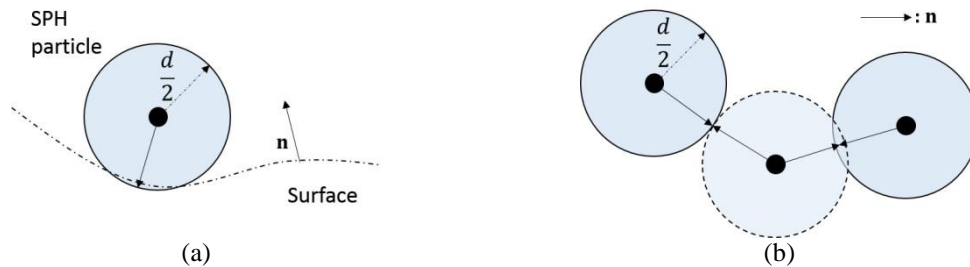


Fig. 4 Contact conditions: (a) particles to surface contact and (b) particle to particle contact

2.2 Numerical models

The submersed rock-berm structure is a typical example on which the SPH method is applicable because rock-berm is a structure constructed by stacking rocks to protect lifelines (e.g., submarine power cables and pipelines). Fig. 5 shows a submersed rock-berm structure consisting of rock particles (the upper layers) modeled by the SPH method and lower seabed (sand) layer modeled by the Lagrange method with 8-node solid elements. The rock-berm structure has the dimensions (lower width 11.1 m, upper width 2.5 m, and height 2.1 m) as shown in Fig. 5.

The rock material model is quite significant for the impact simulation. In the study, the piecewise Drucker-Prager material model was used for the rock layers because the material model is frequently used for the discrete materials such as concrete, rock, and soils (Liu *et al.* 1995, Zhu and Jia 2014). In the rock material model, we used the material properties of Table 1, which is proposed by Chen *et al.* (2000) and the associated pressure-yield stress curve, shown in Fig. 6. As shown, the model represents the pressure-yield behaviours of the rock with a piecewise linear function, constructed using several pressure-yield points.

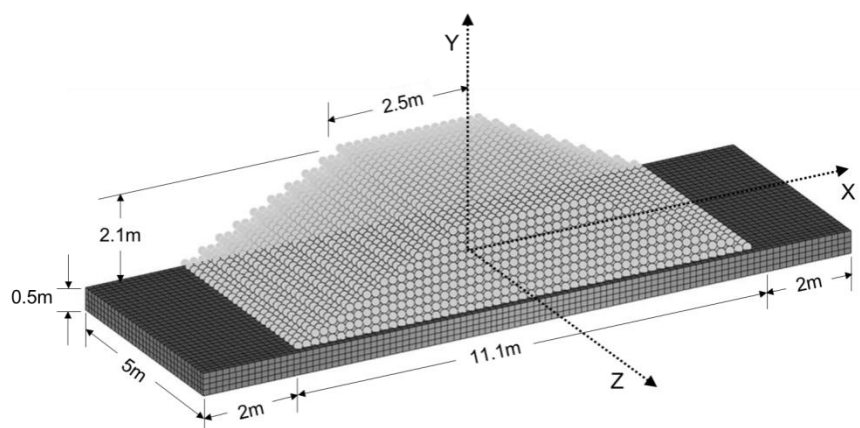


Fig. 5 Model of submersed rock-berm structure

Table 1 Material properties of rock

Parameter	Value	Parameter	Value	Parameter	Value
Density (kg/m ³)	2750	Pressure 1 (MPa)	-30	Yield stress 1 (MPa)	0
Bulk Modulus (GPa)	35.7	Pressure 2 (MPa)	-26.7	Yield stress 2 (MPa)	40
Shear modulus (GPa)	17.44	Pressure 3 (MPa)	200	Yield stress 3 (MPa)	450
Hydro tensile limit (MPa)	30	Pressure 4 (MPa)	1000	Yield stress 4 (MPa)	1430
		Pressure 5 (MPa)	2500	Yield stress 5 (MPa)	2530

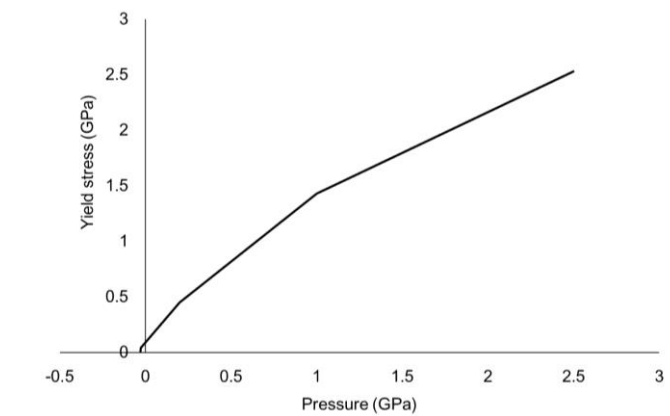


Fig. 6 Pressure-yield stress curve for piecewise Drucker-Prager model

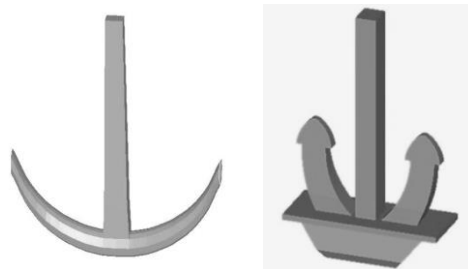


Fig. 7 Anchor models: (a) stock anchor and (b) stockless anchor

Two different anchors (stock and stockless anchors) of 2-ton were modelled according to the KS V 3311 (2012), using four-node shell elements, as shown in Fig. 7. Because of the relatively higher strength than the rocks considered, the anchors were assumed rigid (density 7200 kg/m³). Because the kinetic energy initially occurs to the colliding point and then propagates through the neighbouring rocks, it is believed that the material model of the bottom sand does not have a severe effect on the energy propagation. Thus, the bottom sand was modelled as the linear elastic material (density 2200 kg/m³, Young’s modulus 81 MPa, and Poisson ratio 0.3). The particle (rock) size is fixed to 200 mm, the typical average diameter of the rocks used in the rock-berm structure for protecting submarine power cables.

2.3 Simulation cases

The collision points are located as shown in Fig. 8 such as (1) the center of the upper surface of rock-berm (collision point 1), (2) the side of the upper surface (collision point 2), and (3) the center of slope (collision point 3). For the collision analysis, two impact velocities (terminal velocity and 5 m/s) of each anchor were considered. Here, the terminal velocities of the stock anchor and stockless anchor are known 2.747 m/s and 2.294 m/s, respectively by considering the drag coefficients of the anchors (Woo *et al.* 2013). To determine the effect of impact velocity, an additional velocity 5 m/s was considered. The interval between the anchor and rock-berm is fixed to 20 mm to save the computational time. In the simulation, the vertical displacement of the bottom sand was constrained and the horizontal displacement of the rock-berm was also constrained.

Table 2 shows the simulation cases depending on the collider types (stock and stockless anchor), collision velocities (terminal velocities and 5 m/s), and collision locations (1, 2, and 3). Here, 'Lag' specifies the analysis case using the Lagrange method, and the others denote the analyses using the SPH method. The capital letter 'S' and 'SL' specify the stock anchor and stockless anchor, respectively. The first following number indicates the collision velocity (1: terminal velocities of each anchor and 2: 5 m/s) and the second one represents the collision point (1, 2, and 3). For example, S-11 specifies the stock anchor having 2.774 m/s (terminal velocity) and the collision point 1 (the center of the upper surface of the rock-berm).

3. Results and discussions

Fig. 9(a) is the von-Mises stress distribution of Lag-11. As shown, the von-Mises stress is concentrated on the collision region. Fig. 9(b) shows the von-Mises stress distribution on the cross-section of S-11. As shown, the direction and length of each arrow indicate the direction and size of von-Mises stress. However, it is hard to capture the stress distribution. Therefore, five gauge points were selected to get the response of the simulation. The first point is the bottom of rock-berm and consecutive points were selected with vertical intervals of 500 mm from the first point, as shown in Fig. 8.

Fig. 10 shows the responses of Lag-11 and S-11. According to the analysis method used, the responses show clear distinction. In the S-11, the maximum von-Mises and maximum vertical displacement are generated on the collision region, and the stress and displacement decrease at the lower gauge points. In the Lag-11, the responses look similar to S-11. However, improper stress and displacement are generated. For example, the stress at 0.5 m is smaller than the stress at 0 m, and displacement at 1.5 m is smaller than the results of 0.5 m and 1 m. This is obviously not correct but explainable because of the nature of Lagrange method – each element connected by a shared node unlike SPH. In other words, the coupling between elements and interaction with the bottom boundary conditions cause the incorrect responses. This explanation can be strengthened by the transient time signals, obtained at the gauge points 1, 2, 3, and 4, as shown in Fig. 11. As shown, the results obtained from the Lagrange method include down and up (as indicated by the circles) before reaching the initial peak values. However, the results obtained from the SPH method do not show the down and up trends.

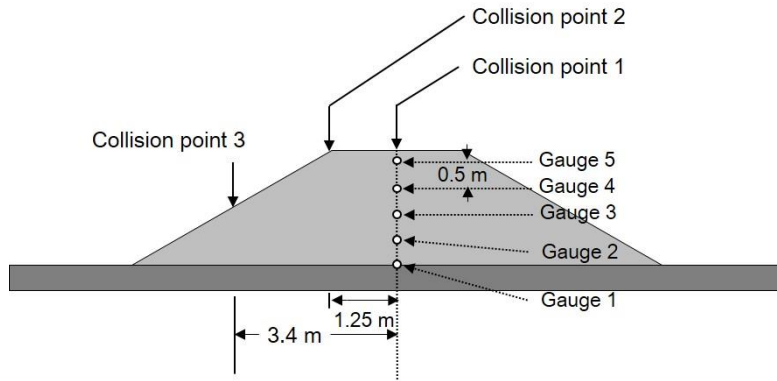


Fig. 8 Locations of collision points and gauge points

Table 2 Simulation cases

Case name	Collider type	Collision velocity	Collision location
Lag-11	Stock anchor	2.774 m/s	1
S-11	Stock anchor	2.774 m/s	1
S-12	Stock anchor	2.774 m/s	2
S-13	Stock anchor	2.774 m/s	3
S-21	Stock anchor	5 m/s	1
S-22	Stock anchor	5 m/s	2
S-23	Stock anchor	5 m/s	3
SL-11	Stockless anchor	2.294 m/s	1
SL-12	Stockless anchor	2.294 m/s	2
SL-13	Stockless anchor	2.294 m/s	3
SL-21	Stockless anchor	5 m/s	1
SL-22	Stockless anchor	5 m/s	2
SL-23	Stockless anchor	5 m/s	3

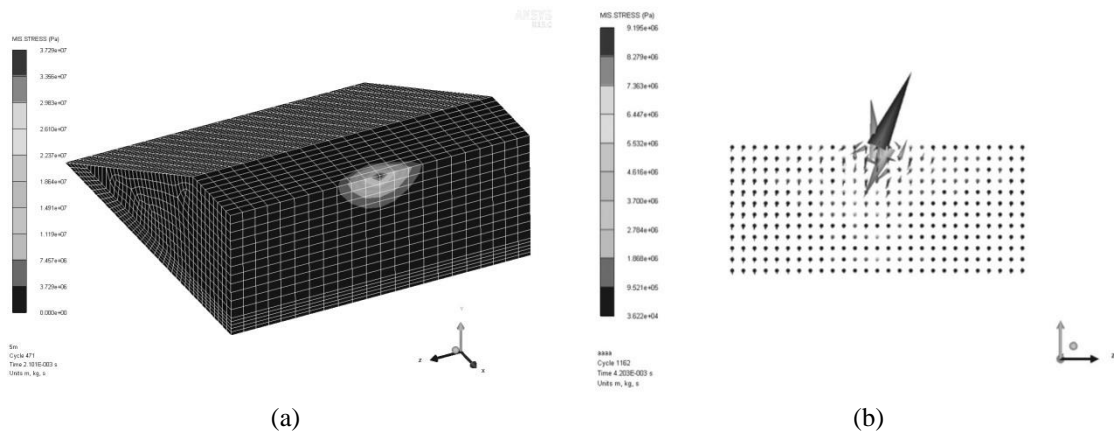


Fig. 9 von-Mises stress contours of (a) Lag-11 and (b) S-11

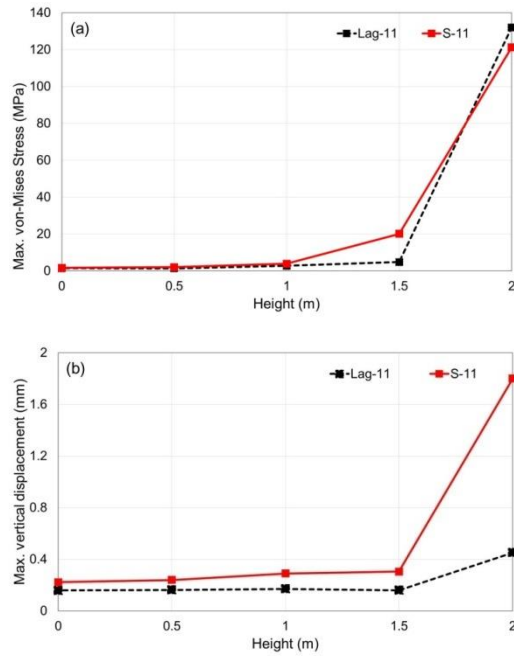


Fig. 10 Responses of Lag-11 and S-11: (a) Max. von-Mises stresses and (b) Max. vertical displacements

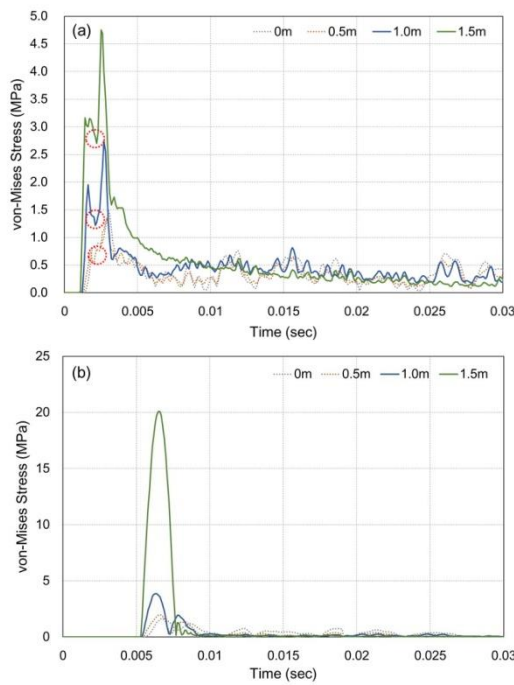


Fig. 11 von-Mises stresses with respect to time in the cases of: (a) Lag-11 and (b) S-11

Fig. 12, Tables 4 and 5 show the responses of the stock anchor cases. To clearly show the differences, the vertical axes are intentionally expressed by the logarithm of the maximum responses. It is shown that, depending on the collision point and velocity, the responses are different. By comparing the result having the same collision point, we can observe that the responses become larger when the collision velocity increases. For example, the response of S-21 (5 m/s) is bigger than S-11 (2.774 m/s). In the case of the collision points 2 and 3, the responses are smaller than those of point 1. Therefore, it is shown that the responses become smaller when the collision points are away from the center of the upper surface of the rock-berm structure. In the case of collision point 2 and 3, the maximum responses did not occur at the highest point. This is because the collision points are not directly on the gauge points. Except for the collision location 1, the stresses and displacements of rock-berm are under 5.1 MPa and 0.376 mm, respectively.

Fig. 13, Tables 4 and 5 show the responses of stockless anchor cases according to the gauge height. To clearly show the differences, the vertical axes are intentionally expressed by the logarithm of the maximum responses. The stresses are different according to the collision point and velocity. By comparing results having the same collision point, we can also observe that the responses become larger when the collision velocity increases. In addition, it is shown that the stresses become smaller when the collision points are away from the center of the upper surface of the rock-berm. An interesting fact is that displacements are similar regardless of the gauge height or location.

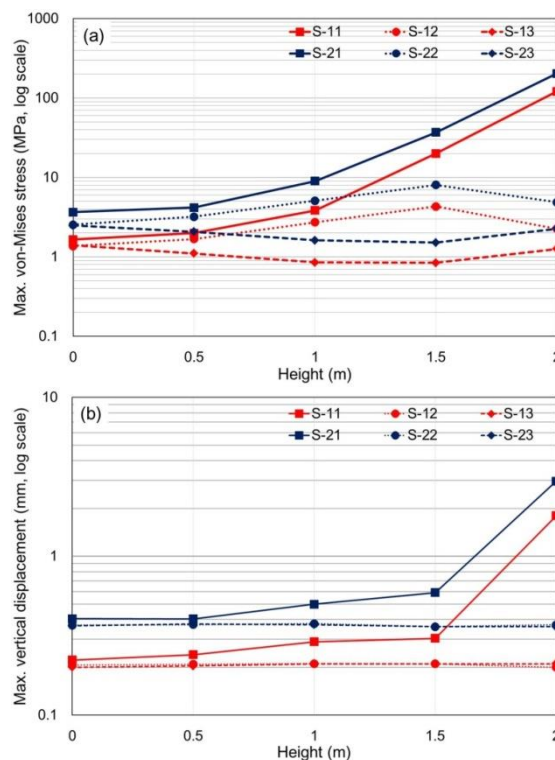


Fig. 12 Responses of the submersed rock-berm structure in the case of stock anchor: (a) Max. von-Mises stresses and (b) Max. vertical displacements

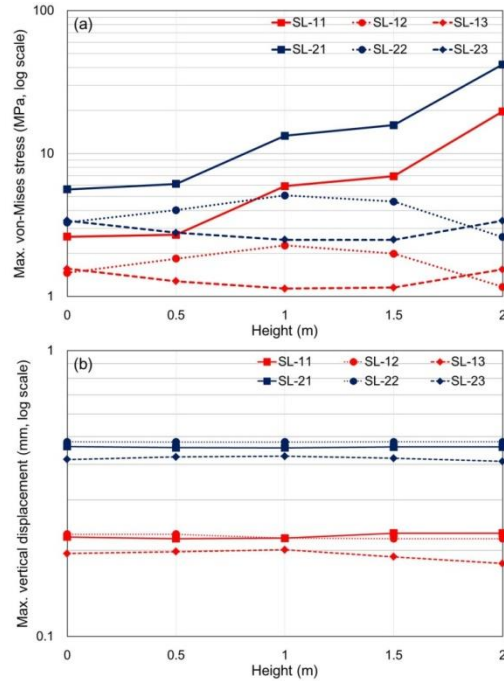


Fig. 13 Responses of the submersed rock-berm structure in the case of stockless anchor: (a) Max. von-Mises stresses and (b) Max. vertical displacements

Table 4 Maximum von-Mises stress of each case (unit: MPa)

	0 m	0.5 m	1 m	1.5 m	2 m
Lag-11	1.49	1.35	2.74	4.75	132
S-11	1.65	2.00	3.85	20.07	121.26
S-12	1.37	1.68	2.73	4.31	2.27
S-13	1.41	1.11	0.85	0.84	1.26
S-21	3.66	4.17	9.01	36.93	203.39
S-22	2.55	3.21	5.10	8.06	4.88
S-23	2.49	2.07	1.61	1.51	2.26
SL-11	2.62	2.70	5.92	6.94	19.74
SL-12	1.46	1.84	2.28	2.00	1.17
SL-13	1.57	1.28	1.14	1.16	1.55
SL-21	5.61	6.14	13.33	15.82	42.05
SL-22	3.30	4.02	5.09	4.62	2.61
SL-23	3.40	2.80	2.49	2.50	3.39

Table 5 Maximum vertical displacement of each case (unit: mm)

	0 m	0.5 m	1 m	1.5 m	2 m
Lag-11	0.159	0.163	0.170	0.160	0.452
S-11	0.222	0.240	0.290	0.304	1.800
S-12	0.206	0.209	0.211	0.210	0.200
S-13	0.200	0.204	0.210	0.210	0.210
S-21	0.405	0.403	0.499	0.590	2.970
S-22	0.368	0.371	0.376	0.360	0.370
S-23	0.364	0.374	0.371	0.360	0.360
SL-11	0.223	0.220	0.221	0.230	0.230
SL-12	0.228	0.228	0.221	0.220	0.220
SL-13	0.195	0.198	0.201	0.190	0.180
SL-21	0.462	0.458	0.457	0.460	0.460
SL-22	0.480	0.479	0.479	0.480	0.480
SL-23	0.416	0.425	0.427	0.420	0.410

Fig. 14 shows the maximum von-Mises stresses according to collision velocity when the collision point is at the center of the upper surface (point 1). The legends show the elevation of the gauge points. For example, the square indicates the elevation (2 m) of the gauge point 5. From the figure, it is shown that the von-Mises stress becomes larger when the collision velocity increases. All the results (Fig. 14(a)) of the stock anchor are bigger than those (Fig. 14(b)) of the stockless anchor because of the difference in the anchor shapes. The stockless anchor has a flatter and wider bottom surface than that of stock anchor; hence, the collision force per unit area of stockless anchor is smaller than that of stock anchor.

It should be noted here that the structural properties of submarine cables are hard to find. Most studies focused on electronic analyses of underwater power cable (Zhang *et al.* 2013, Kalcon *et al.* 2013). According to a study by Tanaka and Kunii (2000), the tensile strength of the modified HDPE cable is 27MPa, and the bending strength is 37MPa. Thus, the stability of underwater power cable was examined using the tensile strength (27 MPa). From the results of von-Mises stresses, the stresses of the gauge points 1, 2, and 3 satisfy the criteria, regardless of the anchor types. This means that the underwater power cable is safe from the anchor collisions (2-ton stock and stockless anchors) when the height of the rock-berm structure is over 1m. It should be noted that this observation holds by assuming the stresses of rocks spread completely to the power cable.

In structural health monitoring point of view, it is desirable to measure the critical stress wave at a certain gauge point. Upon the stress exceeds 27MPa at the gauge point, an alarm system should be implemented. In the practice, the power cable locates just below the gauge point 1, which means the gauge point 1 can be a monitoring point. An alternative candidate is the gauge point 2, 0.5 m above the seabed because a margin is necessary for the power line, which is critical to both of the current ocean energy power transmission and the conventional electric power supply to an island.

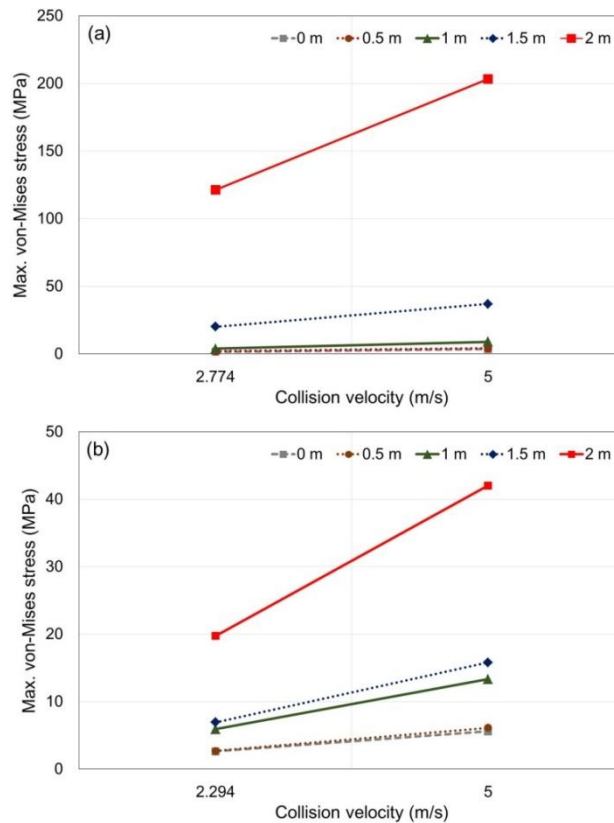


Fig. 14 Max.von-Mises stresses according to collision velocity (collision location: 1): (a) stock anchor and (b) stockless anchor

4. Conclusions

This paper presents the transient dynamic analyses of a submersed rock-berm structure under anchor collision. Two analysis methods (Lagrange and SPH), three collision points, and two collision velocities (terminal velocity of each anchor, and 5 m/s) are considered in the analyses. The responses of the submersed rock-berm structure were measured at five different gauge points. From the numerical simulation, it is found that the SPH method is more suitable for the description of discontinuous material than the Lagrange method because of the following reasons: (1) Lagrange method is not proper to quantify the stresses near the bottom because it does not describe improper stress patterns. (2) Regardless of the anchor type and collision point, the responses of the rock-berm structure become larger when the collision velocity increases. (3) The responses become smaller when the collision points are away from the center of the upper surface of the rock-berm; hence, the gauge points should be located at the center of the structure. Besides, considering the strengths of the modified HDPE (tensile strength 27MPa and bending strength 37MPa), it is shown that the underwater power cable is safe from the anchor collision when the height of the rock-berm is over 1m upon the assumption that the stresses of the rocks completely

propagate to the power cable. Therefore, it is desirable to measure the critical stress wave (27 MPa) at the gauge point 1 (seabed) or the gauge point 2 (0.5 m above the seabed) by implementing a structural health monitoring tool. Considering the significance of submarine power cable, the gauge point 2 gives a margin for structural health monitoring and accordingly better electric power security.

Acknowledgments

This work was supported by a Research Grant of Pukyong National University (2014 year).

References

- Chen, S.G., Zhao, J., Makurati, A. and Madshus, C. (2000), "Discrete element modelling of an explosion test in granite", *Proceedings of the GeoENG2000 International Conference on Geotechnical*, Melbourne, November.
- Coffen-Smout, S. and Herbert, G.J. (2000), "Submarine cables: a challenge for ocean management", *Marine Policy*, **24**, 441-448.
- Corkum, A.G. and Martin, C.D. (2004), "Analysis of a rock slide stabilized with a toe-berm: a case study in British Columbia Canada", *Int. J. Rock Mech. Min.*, **41**(7), 1109-1121.
- Gingold, R.A. and Monaghan, J.J. (1977), "Smoothed particle hydrodynamics: theory and application to non-spherical stars", *Monthly Notice of the Royal Astronomical Society*, **181**, 375-389.
- Hao, Y. and Hao, H. (2013), "Numerical investigation of the dynamic compressive behaviour of rock materials at high strain rate", *Rock Mech. Rock Eng.*, **46**(2), 373-388.
- Hayhurst, C.J., Clegg, R.A., Livingstone, I.H. and Francis, N.J. (1996), "The application of SPH techniques in AUTODYN-2D to ballistic impact problems", *Proceeding of the 16th International Symposium on Ballistics*, San Francisco, September.
- Huynh, T.C., Lee, S.Y., Kim, J.T., Park, W.S. and Han, S.H. (2013), "Simplified planar model for damage estimation of interlocked caisson system", *Smart Struct. Syst.*, **12**(3-4), 441-463.
- International Cable Protection Committee (2009), *Damage to submarine cables caused by anchors*, Loss Protection Bulletin.
- Jie, W. and Yao-Tian, F. (2012), "Study on safety monitoring system for submarine power cable on the basis of AIS and radar technology", *Physics Procedia*, **24**, 961-965.
- Kalcon, G., Adam, G.P., Anaya-Lara, O. and Lo, K.L. (2013), "Analytical efficiency evaluation of two and three level VSC-HVDC transmission links", *Int. J. Elec. Power*, **44**(1), 1-6.
- Kim, J.K., Woo, J. and Na, W.B. (2008), "Finite element simulation of two-point elastic wave excitation method for damage detection in concrete structures", *Russ. J. Nondestruct. T.*, **44**(10), 719-726.
- KS V 3311 (2012), *Anchors*, Korean Standard.
- Lee, S.Y., Nguyen, K.D., Huynh, T.C., Kim, J.T., Yi, J.H. and Han, S.H. (2012), "Vibration-based damage monitoring of harbor caisson structure with damaged foundation-structure interface", *Smart Struct. Syst.*, **10**(6), 517-546.
- Li, H.N., Yi, T.H., Ren, L., Li, D.S. and Huo, L.S. (2014), "Reviews on innovations and applications in structural health monitoring for infrastructures", *Struct. Monit. Maint.*, **1**(1), 1-45.
- Libersky, L.D. and Petschek, A.G. (1991), "Smooth particle hydrodynamics with strength of materials", in *Advances in the Free-Lagrange Method Including Contributions on Adaptive Gridding and the Smooth Particle Hydrodynamics Method*, *Lecture Notes in Physics*, 248-257, Springer, Berlin, Germany.
- Lin, J., Naceur, H., Coutellier, D. and Laksimi, A. (2014), "Efficient meshless SPH method for the numerical modeling of thick shell structures undergoing large deformations", *Int. J. Nonlinear Mech.*, **64**,

1-13.

- Liu, W.K., Jun, S., Li, S., Adee, J. and Belytschko, T. (1995), "Reproducing kernel particle methods for structural dynamics", *International Journal of Numerical Methods in Engineering*, **38**(10), 1655-1679.
- Lucy, L.B. (1977), "A numerical approach to the testing of the fission hypothesis", *Astronomical J.*, **82**, 1013-1024.
- Na, W.B. and Kundu, T. (2002), "Underwater pipeline inspection using guided waves", *J. Pressure Vessel Technol. – T. ASME*, **124**(2), 196-200.
- Na, W.B. and Yoon, H.S. (2007), "Parametric density concept for long-range pipeline health monitoring", *Smart Struct. Syst.*, **3**(3), 357-372.
- Ren, P. and Zhou Z. (2012), "A state-of-the-art review on structural health monitoring of deepwater floating platform", *Pacific Sci. Rev.*, **14**(3), 253-263.
- Sasalone, M. (1997), "Impact-echo: the complete story", *ACI Struct. J.*, **94**, 777-786.
- Sasalone, M. and Carino, N.J. (1987), "Transient impact response of plates containing flaws", *J. National Bureau of Standards*, **92**, 369-381.
- Seo, S. and Min, O. (2006), "Axisymmetric SPH method of elasto-plastic contact in the low velocity impact", *Comput. Phys. Commun.*, **175**, 583-603.
- Tanaka, T. and Kunii, K. (2000), "High performance HVDC polymer cable", *Fujikura Technical Review*, **29**, 57-62.
- Tørum, A., Moghim, M.N., Westeng, K., Hidayati, N. and Arntsen, Ø. (2012), "On berm breakwaters: Recession, crown wall wave forces, reliability", *Costal Eng.*, **60**, 299-318.
- Wagner, E. (1995), "Submarine cables and protections provided by the law of the sea", *Marine Policy*, **19**, 127-136.
- Woo, J. and Na, W.B. (2014), "Drag coefficients of stock and stockless anchors", *Marine Technol. Soc. J.*, **48**(3), 138-145.
- Woo, J., Na, W.B. and Kim, H.T. (2009), "Numerical simulation of arch-type submarine cable protector under anchor collision", *J. Ocean Eng. Technol.*, **23**, 96-103.
- Woo, J., Na, W.B. and Yu, J.S. (2013), "Analysis of the falling velocity of underwater anchor using computational fluid dynamics", *Proceedings of the Korean Association of Ocean Science and Technology Joint Workshop*, JeJu, May.
- Yang, Y., Annamdas, V.G.M., Wang, C. and Zhou, Y. (2008), "Application of multiplexed FBG and PZT impedance sensors for structural health monitoring of rocks", *Sensors*, **8**, 271-289.
- Yi, J.H., Kim, J.H., Jeong, W.M. and Chae, J.W. (2013a), "Field evaluation of optical-based three-dimensional dynamic motion measurement system with multiple targets for a floating structure", *Ocean Eng.*, **62**, 140-151.
- Yi, J.H., Park, J.S., Han, S.H. and Lee, K.S. (2013b), "Modal identification of a jacket-type offshore structure using dynamic tilt responses and investigation of tidal effects on modal properties", *Eng. Struct.*, **49**, 767-781.
- Yoon, H.S. and Na, W.B. (2013a), "Anchor drop tests for a submarine power-cable protector", *Marine Technol. Soc. J.*, **47**(3), 72-79.
- Yoon, H.S. and Na, W.B. (2013b), "Safety assessment of submarine power cable protectors by anchor dragging field tests", *Ocean Eng.*, **65**, 1-9.
- Zhang, X., Bai, J., Cao, G. and Chen, C. (2013), "Optimizing HVDC control parameters in multi-infeed HVDC system based on electromagnetic transient analysis", *Int. J. Elec. Power*, **49**, 449-454.
- Zhu, X.H. and Jia, Y.J. (2014), "3D mechanical modeling of soil orthogonal cutting under a single reamer cutter based on Drucker-Prager criterion", *Tunneling and Underground Space Technology*, **41**, 255-262.
- Zhu, Z., Mohanty, B. and Xie, H. (2007), "Numerical investigation of blasting-induced crack initiation and propagation in rocks", *Int. J. Rock Mech. Min.*, **44**(3), 412-424.